Magnetic hopfions in toroidal nanostructures driven by an Oersted magnetic field

S. Castillo-Sepúlveda⬤

Departamento de Ingeniería, Universidad Autónoma de Chile, Avenida Pedro de Valdivia 425, Providencia, Chile

R. Cacilhas⬤ and V. L. Carvalho-Santos⬤

Departamento de Física, Universidade Federal de Viçosa, Avenida Peter Henry Rolfs s/n, 36570-000 Viçosa, Minas Gerais, Brazil

R. M. Corona⬤ and D. Altbir⬤

Departamento de Física, CEDENNA, Universidad de Santiago de Chile, Avenida Ecuador 3493, Santiago, Chile

The search for magnetic hopfions has been the focus of intense research during the last years. In this direction, and using micromagnetic simulations, we studied the magnetization reversal mechanism in toroidal nanoparticles under the action of an Oersted magnetic field. Our results evidence the nucleation of four magnetic configurations as a function of geometry, two of them being hopfion-like textures. These mechanisms are preferred for large toroidal structures. The annihilation of such texture is indicated by strong changes in the energy, which characterizes a topological transition.

I. INTRODUCTION

Current experimental techniques to fabricate magnetic nanoparticles have made it possible to produce nanomagnets with a large variety of shapes and sizes [1–5]. These new techniques promote an expansion of three-dimensional nanomagnetism, leading to the appearance of a new class of magnetic effects that cannot be observed in planar or quasi-one-dimensional structures [4]. Among the 3D emergent collective modes of magnetization one can highlight the possibility to stabilize confined skyrmion tubes [6], the formation of magnetic vortex rings [7], the appearance of topological defects in a double helix of nanowires [8], and the nucleation of topological objects such as Bloch points [9,10] and hopfions [11]. In addition to the nucleation of new magnetic textures, advances in nanomagnet fabrication opens up the possibility of using ferromagnetic nanoparticles as components of memory devices [12], data storage [13], sensors [14,15], cancer therapy [16], nano-oscillators [17,18], and neuromorphic computing [19–21]. These applications are based on new magnetoelectronic behaviors that these nanostructures exhibit, and demand a profound knowledge and control of the magnetization and the existence of stable magnetic configurations in a magnetic element at the nanoscale.

For such applications it is fundamental to understand the role of geometry on the dynamics and static properties of a magnetic nanostructure [4,22,23]. In this direction, structures with cylindrical symmetry such as nanodisks, nanorings, nanowires, and nanotubes have been intensely studied [24–30]. Such geometries exhibit interesting magnetic phenomena, such as the displacement of domain walls by electric currents and magnetoresistance [31–35]. Particularly, from an applications point of view, a good control of the

magnetization ground state in nanorings [28] allows their use in random access memory devices [36–38]. One remarkable feature is that the presence of a central hole allows nanorings to host magnetic vortices as the ground state for smaller sizes than cylindrical nanodots. These vortices are characterized by a chirality, defined as the rotation direction of the magnetization vector field, which can be reversed by Oersted fields [39,40].

The properties of magnetic nanorings with a torus-like geometry and topology have been also studied in several works. Although cylindrical rings share the torus topology (cylindrical rings can be continuously deformed in a torus), both geometries present subtle differences. For instance, while the torus presents a Gaussian curvature that changes smoothly from negative to positive when one goes from the internal to the external border, the Gaussian curvature of cylindrical nanorings vanishes in the whole surface and is not well defined at the borders. Additionally, theoretical predictions show a broad class of new phenomena that makes the toroidal geometry a very interesting object in 2D and 3D nanomagnetism, such as the fact that they can accommodate a vortex as the ground state for a smaller external radius than cylindrical nanorings [41–43]. It was also shown that the appearance of a geometrical frustration associated with the torus geometry (toroidal and poloidal radii) leads to soliton instability [44,45]. Because purely in-surface states in ferromagnetic shells cannot be stabilized [46], deviation from the in-surface vortex configuration results in the development of an out-of-surface vortex core [47]. When an in-plane uniaxial magnetic field is applied, the reversal of the magnetization occurs through two different modes, coherent rotation or vortex nucleation [42]. Nevertheless, the magnetization reversal in a toroidal shell with a large aspect ratio ($\xi = r/R$) occurs by forming
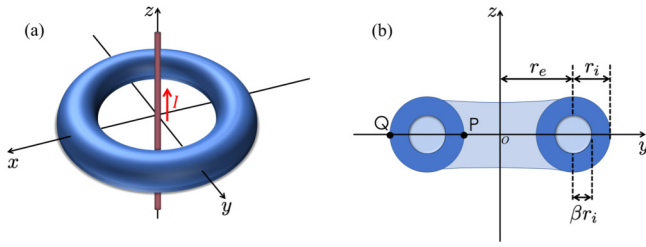
FIG. 1. (a) Schematic representation of a toroidal tube, with an inner conductor wire in the z axis along which an electric current flows. (b) yz plane of the torus, illustrating P and Q, which represent the inner and outer radii of the toroid, respectively. The geometrical parameters r_e and r_i describe the toroidal and poloidal radii, respectively, and β defines the tube thickness.

a vortex-antivortex pair as a remanent state, where the vortex and the antivortex are nucleated in the region with positive and negative curvatures, respectively [48]. This curvature-induced winding number selection is intrinsically related to effective geometry-induced interactions [46,49–52].

In this work, through micromagnetic simulations, we investigate the magnetization reversal modes of ferromagnetic nanotori under the action of an azimuthal magnetic field. Our main focus is to find the reversal modes and search for the appearance of hopfions, which are field configurations localized in all three spatial dimensions that maps a three-sphere S^3 to the order parameter space S^2, belonging to the third homotopy group [11,53] $\pi_3(S_2) = \mathbb{Z}$. Our results have revealed that depending on the torus geometry the magnetization is driven by the nucleation and propagation of four reversal modes consisting of 3D emergent magnetic structures depending on the geometrical parameters: a hopfion structure, a pinned-hopfion texture, an almost coherent reversion [47], and transversal radial walls. It is worth noticing that hopfions have been predicted to appear in chiral magnetic systems presenting helical or conical order [54]. In the present case, the observed hopfion structures are obtained even in the absence of Dzyaloshinskii-Moriya interactions (DMIs), and only as a result of the magnetostatic and exchange competition, similarly to the nucleation of skyrmions in nanodots without DMIs [55]. Hopfion-like reversal modes are interesting emergent objects in 3D magnetism since they represent collective modes of the magnetization belonging to specific homotopy sectors in a 3D space. Therefore, these magnetic quasiparticles have topological stability and have been considered as information carriers [56].

This work is organized as follows: Section II describes the micromagnetic simulations used in this work. Section III presents our results for the hysteresis curves and a discussion on the reversal modes. Finally, Sec. IV contains conclusions.

II. MICROMAGNETIC SIMULATION

In our work we study the reversal modes of a toroidal tube using Object Oriented MicroMagnetic Framework (OOMMF) simulations [57]. The hollow torus is characterized by the toroidal (r_e) and poloidal (r_i) radii, respectively, as illustrated in Fig. 1. The thickness of the tube cross section is defined as $t = (1 − \beta)r_i$, where $\beta \in [0, 1)$ determines the thickness

of the tube, from a toroidal shell ($\beta \to 1$) to a solid toroid ($\beta = 0$). In the simulations we consider a fixed toroidal radius of $r_e = 100$ nm and a poloidal radius r_i that varies from 20 to 80 nm in 10 nm steps, while β varies from 0.0 to 0.8. The magnetization reversal is driven by an Oersted field, which can be generated, in an experimental setup, by an electric current in a conductor wire oriented parallel to the torus axis passing through the nanotorus center [see Fig. 1(a)].

The magnetic parameters used in the simulations are the exchange constant $A = 13 \times 10^{-12}$ J m^{-1} and saturated magnetization $M_s = 860 \times 10^3$ A m^{-1}. These parameters represent permalloy (Py), a soft magnetic material that permits us to neglect the magnetocrystalline anisotropy allowing us to observe in a better way the contribution of the geometric parameters. The magnetic energy is given by $E = E_{ex} + E_{ms} + E_Z$, where E_{ex}, E_{ms}, and E_Z are the exchange, magnetostatic, and Zeeman energies, respectively. In all the simulations we consider cell sizes of $2 \times 2 \times 2$ nm^3, which are small enough with respect to the Py exchange length and generate a structure with smooth curvature in such a way that border effects can be neglected. To study the magnetization reversal modes we use a damping constant equal to 0.5. The external Oersted field H_{Oe} is radially nonhomogeneous, with its magnitude decreasing as a function of R (the cylindrical radial distance). The electrical current in the wire, I, is varied between 0.125 and -0.125 A, inducing a circular Oersted field in the azimuthal direction with a maximum value of $\mu_0 H_{max} = 350$ mT. Our results are valid for isolated elements as well as for arrays in which the inter-element distance is large enough to consider each element as a noninteracting one.

III. RESULTS

We start by obtaining the hysteresis curves for the nanotorus under the action of an induced circular Oersted field for different β values and for poloidal radius $r_i = 20$, 40, and 80 nm. Here, we consider that $m_\phi = 1$ when the magnetization consists of a vortex swirling counterclockwise and $m_\phi = -1$ when it is clockwise. The hysteresis curves are depicted in Fig. 2, where one can notice that all cycles exhibit a square shape with a single jump. We also note that the coercive field strongly depends on both β and r_i. Hysteresis loops with different areas result from the different works needed to reverse the orientation of the magnetic moments [58]. Therefore, our results show that the magnetization reversal of a solid toroid with a large poloidal radius demands more energy than a thin toroidal tube with a small poloidal radius.

From the hysteresis curves, it is possible to determine the coercive field of the toroidal tube as a function of β and r_i. Figure 3 summarizes the obtained results, from which one can notice a linear decrease of the coercive field as a function of r_i for fixed β as well as a decrease in the slope of the curve as a function of β for fixed r_i. In the first case, coercive fields practically converge for $r_i = 80$ nm independently of β [see Fig. 3(a)]. On the other hand, Fig. 3 shows that the dependence of the coercive field on r_i for a specific β is not a linear function.

To better understand this behavior we analyze the magnetization reversal for the toroidal tube. In Fig. 4 we show some snapshots of the reversal process revealing that in the
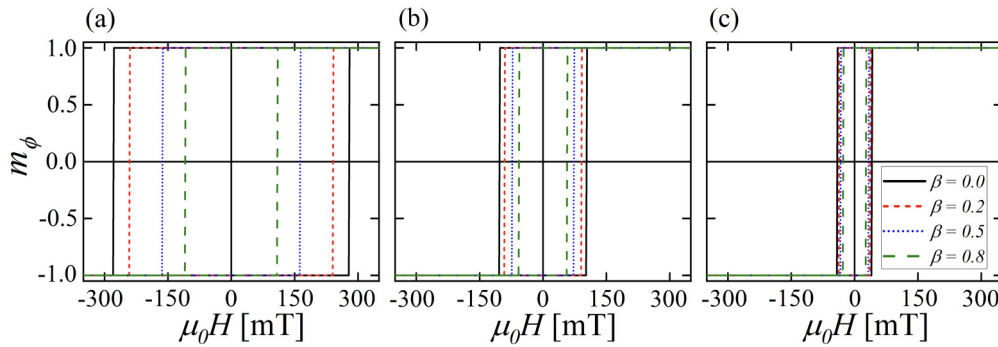
FIG. 2. Hysteresis curves for $\beta = 0.0$, 0.2, 0.5, and 0.8 values for (a) $r_i = 20$ nm, (b) $r_i = 40$ nm, and (c) $r_i = 80$ nm.

systems under study the reversion occurs through four different mechanisms as a function of β and r_i. The first is hopfion nucleation, that is, a state consisting of a skyrmion tube closed in on itself due to the constraints of the toroidal geometry. It is important to notice that the hopfion is nucleated even in the absence of an intrinsic DMI, as result of the competition between exchange and dipolar interactions, similarly to the nucleation of skyrmions in nanodots without DMIs [55]. To ensure that the observed state consists of a hopfion, we have plotted the magnetization pattern of a very thin disk taken off of the torus cross section [see Fig. 4(b)]. One can notice that the observed pattern is a 2D skyrmion. In Fig. 5 we illustrate the other three reversal modes. Figure 5(a) shows the pinned-hopfion mechanism, where the reversal process is mediated by the formation of a hopfion with a noninteger hopfion topological index. In this case, the 3D skyrmion center is pinned at the toroid central hole, forming a noninteger skyrmion tube closed in on itself. Figure 5(b) depicts a quasicoherent fast reversion, mediated by the formation of a quasitangential poloidal vortex. That is, the magnetic moments rotate around the poloidal radial direction. The poloidal vortex state is not completely tangent to the surface because purely tangential states cannot appear in curved magnetic surfaces [46]. Figure 5(c) illustrates the nucleation of two transversal radial domain walls that propagate radially along the torus cross section. These four reversal processes involve the appearance

of a cross-vortex component m_{ϑ} of the magnetization, forming nice 3D emergent structures in magnetic nanotori. See the Supplemental Material [59] for videos showing the full magnetization reversal process for the hopfion, pinned-hopfion, transversal radial wall, and quasicoherent mechanisms. Time is in nanoseconds.

Aiming at determining the geometrical phase space at which hopfions can be nucleated we performed a series of micromagnetic simulations, obtaining a map of the reversal mechanisms as a function of β and r_i. The obtained results are presented in Fig. 6, where blue circles indicate the regions where the reversion is given by the nucleation of hopfions, green squares represent the pinned hopfion, pink stars represent the quasicoherent rotation, and orange diamonds represent the range of parameters for which the nucleation of transversal radial walls appear.

The analysis of the reversal modes as a function of the toroidal geometrical parameters reveals that toroids with higher values of β present a magnetization reversal driven by the nucleation of two domain walls at point P. These domain walls displace along with opposite directions and annihilate themselves at Q (see Fig. 1). This mode appears when there is not enough material allowing the nucleation of swirling 3D magnetization patterns. Reversal mechanisms mediated by domain wall creation and annihilation are also observed in magnetic nanorings [35], but in that context, the domain
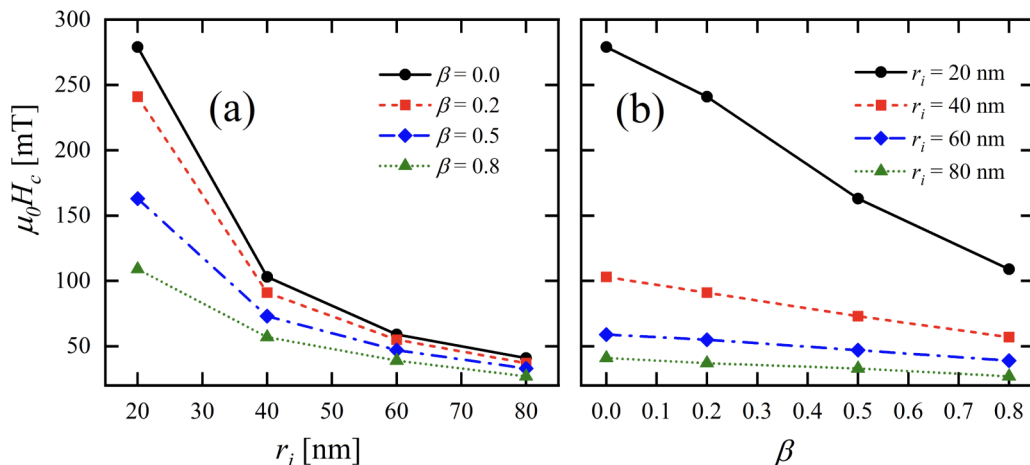

FIG. 3. Coercive field as a function of (a) r_i for some fixed β values and (b) β for some fixed r_i values.
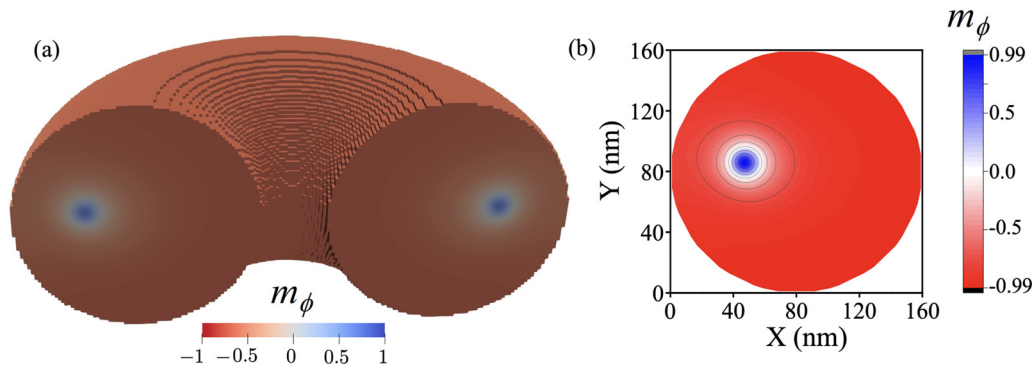
FIG. 4. Snapshots of the hopfion-mediated magnetization reversal process. Blue represents the region where $m_\phi = 1$ and red depicts the internal vortex in the opposite direction $m_\phi = -1$.

walls propagate along the wire length while in the present study, since we use a radial magnetic field, the domain walls propagate along the ϑ direction of the torus, without variation in φ.

Nevertheless, by increasing r_i and decreasing β there is enough volume in the magnetic body to nucleate more complex magnetic textures. Our results give evidence for hopfions—and pinned hopfions—for $\beta \lesssim 0.4$, requiring larger r_i for larger β values. These magnetic textures exist because of the radial nature of the field along the azimuthal direction of the torus, decreasing as $1/r$. It is worth noticing that the damping constant α controls the range of fields for which the hopfion exists in a metastable state. Lower α values create hopfions that are annihilated fast, or that may not even be observed if larger time steps are used.

The obtained hopfion state can be viewed as a chain of skyrmions hosted in 2D nanodots that close in on themselves, forming a toroidal structure. Skyrmions can appear as stable states in 2D dots with uniaxial magnetic anisotropy even in the absence of DMIs [55]. However, once we close the chain in on itself, this uniaxial anisotropy is no longer needed since it naturally appears as a shape anisotropy that forces the magnetization to point along the azimuthal direction. In this context, the obtained 3D magnetization profile consists of a skyrmion tube closed in on itself. The pinned-hopfion state appears when the central hole of the tube pins the vortex with opposite chirality. Similarly to the nucleation of hopfions, this magnetization profile can be promptly understood if we interpret the pinned-hopfion profile in a toroidal cross section as a half-skyrmion hosted in 2D magnetic rings [60]. The pinning mechanism can be understood in the same way that vortices and skyrmions in nanorings are pinned by the hole for large values of the internal radius [61–63]. The high energy cost to nucleate hopfions and pinned hopfions is evidenced
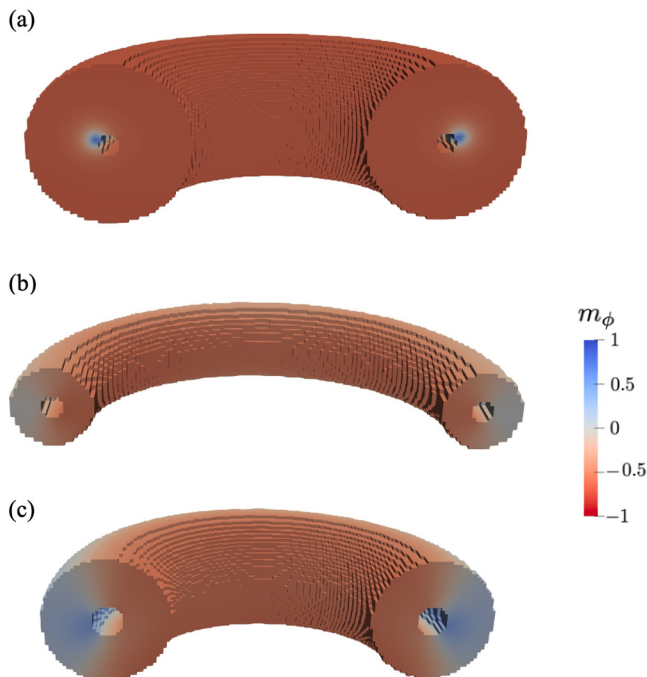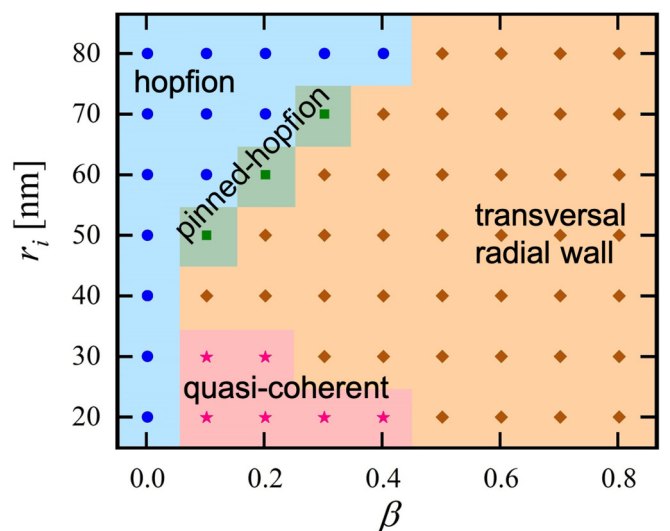

FIG. 5. Snapshots of the (a) pinned-hopfion, (b) transversal radial wall, and (c) quasicoherent magnetization reversal processes. Blue represents the region where $m_\phi = 1$ and red depicts the region with $m_\phi = -1$.

FIG. 6. Phase diagram of the reversal mechanisms for different values of r_i and β. Blue circles, green squares, pink stars, and orange diamonds represent respectively the regions where the reversal process is mediated by hopfion, pinned-hopfion, quasicoherent wall, and transversal wall nucleation mechanisms.
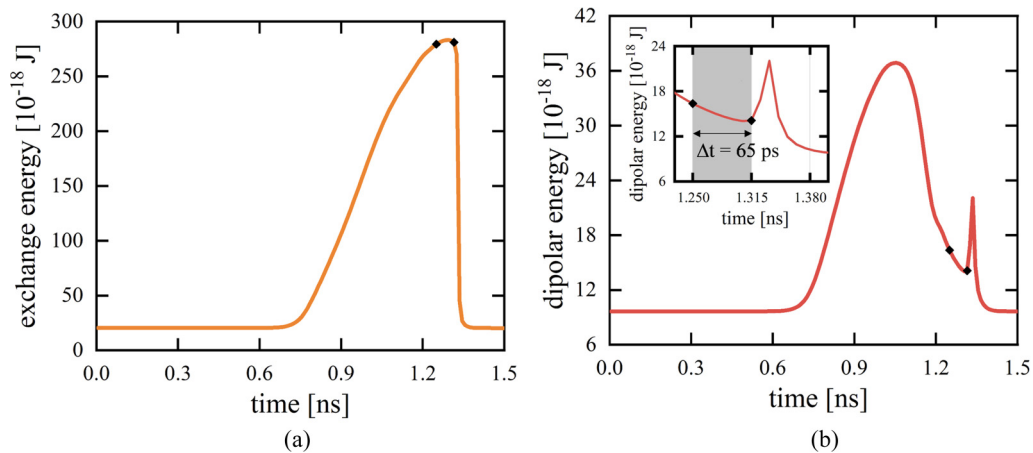
FIG. 7. (a) Exchange and (b) dipolar energies during the hopfion-mediated reversal process.

from the observed greater area of the hysteresis curve [58] for large poloidal radius and small values of β (see Fig. 2). It is also worth noticing that the possibility of the nucleation of hopfions into tori structures was pointed out in Ref. [64], where the authors obtained the hopfion's circle preimages, showing that it resides on a nested torus embedded in a 3D space. Nevertheless, in that work, due to the presence of a uniaxial anisotropy and absence of dipolar energy, the vector field of the far-field background points along the z-axis direction. In the present study, due to dipolar interactions, the torus geometry yields a constraint in the magnetization vector field, which points quasitangentially along the azimuthal direction. Therefore, even in the case of a torus with large radius, the far-field background would be on a rotational vector field.

An interesting point to be highlighted is the behavior of magnetic energy during the hopfion-mediated reversal process. Figure 7 depicts exchange and dipolar energies during the reversion of the magnetization of a torus with $r_i = 80$ nm and $\beta = 0.0$. It can be noticed that the hopfion texture nucleation increases the exchange energy due to the formation of a swirling texture along the torus cross section (see Fig. 7). During the nucleation process, the dipolar energy presents a nonmonotonic behavior [see Fig. 7(b)]. An increase in the dipolar energy is observed due to the formation of surface and volumetric magnetic charges during the beginning of the hopfion nucleation. Nevertheless, just before the complete hopfion is nucleated, the formation of a swirling spin texture along the torus cross section yields the surface magnetic charges vanishing, leading to an abrupt drop in the dipolar energy until the hopfion is fully created [the region between the black dots in Fig. 7(b)]. Despite this energy drop, the dipolar energy of the hopfion configuration is still higher than that of an in-surface magnetization state. Therefore, unlike their 2D counterparts (skyrmions in nanodots), the hopfions nucleated in magnetic nanotori are a transient state that appears just in the case of a large poloidal radius, which allows enough space to nucleate a swirling spin texture along the cross section of the torus. Indeed, the energy associated with this swirling magnetization profile would have a very high exchange cost if nucleated in nanotori with a small poloidal radius. Finally,

because the external magnetic field decreases as a function of r, the hopfion center displaces to the border of the torus. Therefore, during the hopfion annihilation it is possible to observe an abrupt reduction in the exchange energy and a bump in the dipolar term. This abrupt change in the energy is characteristic of a topological phase transition, when the hopfion pattern decays to the in-surface state (see Figs. 4 and 5, and the Supplemental Material [59]).

IV. CONCLUSION

In conclusion, we studied the magnetization reversal mechanism in toroidal nanoparticles under the action of an Oersted magnetic field. Micromagnetic simulations allowed us to obtain a phase diagram of the possible reversal processes. Depending on the geometrical parameters of the torus four main mechanisms are responsible for the magnetization reversal. Among these mechanisms, there are two that include the creation and annihilation of hopfion-like textures. It is worth noticing that the observed hopfion structures are obtained even in the absence of Dzyaloshinskii-Moriya interactions (DMIs), as a result of the magnetostatic and exchange competition under an azimuthal magnetic field. Hopfion-like reversal modes are interesting emergent objects in 3D magnetism since they represent collective modes of the magnetization belonging to specific homotopy sectors in a 3D space. Therefore, these magnetic quasiparticles have topological stability and have been considered as information carriers [56]. Our results allow us to determine the time during which these structures exist.

[1] H. Kloust, R. Zierold, J. P. Merkl, C. Schmidtke, A. Feld, E. Poselt, A. Kornowski, K. Nielsch, and H. Weller, Chem. Mater. **27**, 4914 (2015).

[2] M. S. Islam, Y. Kusumoto, and M. Abdulla-Al-Mamun, Mater. Lett. **66**, 165 (2012).

[3] C.-J. Jia, L.-D. Sun, F. Luo, X.-D. Han, L. J. Heyderman, Z.-G. Yan, C.-H. Yan, K. Zheng, Z. Zhang, M. Takano, N. Hayashi, M. Eltschka, M. Kläui, U. Rüdiger, T. Kasama, L. Cervera-Gontard, R. E. Dunin-Borkowski, G. Tzvetkov, and J. Raabe, J. Am. Chem. Soc. **130**, 16968 (2008).

[4] A. Fernaández-Pacheco, R. Streubel, O. Fruchart, R. Hertel, P. Fischer, and R. P. Cowburn, Nat. Commun. **8**, 15756 (2017).

[5] D. D. Sheka, Appl. Phys. Lett. **118**, 230502 (2021).

[6] M. T. Birch, D. Cortés-Ortuño, L. A. Turnbull, M. N. Wilson, F. Groß, N. Träger, A. Laurenson, N. Bukin, S. H. Moody, M. Weigand, G. Schütz, H. Popescu, R. Fan, P. Steadman, J. A. T. Verezhak, G. Balakrishnan, J. C. Loudon, A. C. Twitchett-Harrison, O. Hovorka, H. Fangohr, F. Y. Ogrin *et al.*, Nat. Commun. **11**, 1726 (2020).

[7] C. Donnelly, K. L. Metlov, V. Scagnoli, M. Guizar-Sicairos, M. Holler, N. S. Bingham, J. Raabe, L. J. Heyderman, N. R. Cooper, and Sebastian Gliga, Nat. Phys. **17**, 316 (2021).

[8] D. Sanz-Hernándes, A. Hierro-Rodriguez, C. Donnelly, J. Pablo-Navarro, A. Sorrentino, E. Pereiro, C. Magén, S. McVitie, J. M. de Teresa, S. Ferrer, P. Fischer, and A. Fernández-Pacheco, ACS Nano **14**, 8084 (2020).

[9] S. Da Col, S. Jamet, N. Rougemaille, A. Locatelli, T. O. Mentes, B. S. Burgos, R. Afid, M. Darques, L. Cagnon, J. C. Toussaint, and O. Fruchart, Phys. Rev. B **89**, 180405(R) (2014).

[10] C. Donnelly, M. Guizar-Sicairos, V. Scagnoli, S. Gliga, M. Holler, J. Raabe, and L. J. Heyderman, Nature (London) **547**, 328 (2017).

[11] Jung-Shen B. Tai and I. I. Smalyukh, Phys. Rev. Lett. **121**, 187201 (2018).

[12] C. I. L. de Araujo, S. G. Alves, L. D. Buda-Prejbeanu, and B. Dieny, Phys. Rev. Appl. **6**, 024015 (2016).

[13] S. Parkin and S.-H. Yang, Nat. Nanotechnol. **10**, 195 (2015).

[14] J. Dai, J.-Q. Wang, C. Sangregorio, J. Fang, E. Carpenter, and J. Tang, J. Appl. Phys. **87**, 7397 (2000).

[15] S. H. Sun, C. B. Murray, D. Weller, L. Folks, and A. Moser, Science **287**, 1989 (2000).

[16] D.-H. Kim, E. Rozhkova, I. Ulasov, S. Bader, T. Rajh, M. Lesniak, and V. Novosad, Nat. Mater. **9**, 165 (2009).

[17] E. Bankowski, T. Meitzler, R. S. Khymyn, V. S. Tiberkevich, A. N. Slavin, and H. X. Tang, Appl. Phys. Lett. **107**, 122409 (2015).

[18] O. O. Toro, S. G. Alves, V. L. Carvalho-Santos, and C. I. L. de Araújo, J. Appl. Phys. **127**, 183905 (2020).

[19] J. Torrejon, M. Riou, F. A. Araujo, S. Tsunegi, G. Khalsa, D. Querlioz, P. Bortolotti, V. Cros, K. Yakushiji, A. Fukushima, H. Kubota, S. Yuasa, M. D. Stiles, and J. Grollier, Nature (London) **547**, 428 (2017).

[20] J. Grollier, D. Querlioz, K. Y. Camsari, K. Everschor-Sitte, S. Fukami, and M. D. Stiles, Nat. Electron. **3**, 360 (2020).

[21] T. Blachowicz and A. Ehrmann, Molecules **25**, 2550 (2020).

[22] R. Streubel, P. Fischer, F. Kronast, V. P. Kravchuk, D. D. Sheka, Y. Gaididei, O. G. Schmidt, and D. Makarov, J. Phys. D **49**, 363001 (2016).

[23] E. Y. Vedmedenko, R. K. Kawakami, D. D. Sheka, P. Gambardella, A. Kirilyuk, A. Hirohata, C. Binek, O. Chubykalo-Fesenko, S. Sanvito, B. J. Kirby, J. Grollier, K. Everschor-Sitte, T. Kampfrath, C.-Y. You, and A. Berger, J. Phys. D: Appl. Phys. **53**, 453001 (2020).

[24] S. H. Chung, R. D. McMichael, D. T. Pierce, and J. Unguris, Phys. Rev. B **81**, 024410 (2010).

[25] W. Scholz, K. Y. Guslienko, V. Novosad, D. Suess, T. Schrefl, R. W. Chantrell, and J. Fidler, J. Magn. Magn. Mater. **266**, 155 (2003).

[26] D. Gregurec, A. W. Senko, A. Chuvilin, P. D. Reddy, A. Sankararaman, D. Rosenfeld, P.-H. Chiang, F. Garcia, I. Tafel, G. Varnavides, E. Ciocan, and P. Anikeeva, ACS Nano **14**, 8036 (2020).

[27] H. Gao, T. Zhang, Y. Zhang, Y. Chen, B. Liu, J. Wu, X. Liu, Y. Li, M. Peng, Y. Zhang, G. Xie, F. Zhao, and H. M. Fan, J. Mater. Chem. B **8**, 515 (2020).

[28] P. Landeros, J. Escrig, D. Altbir, M. Bahiana, and J. d'Albuquerque e Castro, J. Appl. Phys. **100**, 044311 (2006).

[29] M. Vázquez, Advanced magnetic nanowires, in *Handbook of Magnetism and Advanced Magnetic Materials*, edited by H. Kromüller and S. Parkin (Wiley, Chichester, 2007), Vol. 4.

[30] M. Stano and O. Fruchart, Magnetic nanowires and nanotubes, in *Handbook of Magnetic Materials* (Elsevier, North Holland, 2018), Vol. 27, pp. 155–267.

[31] A. L. Gonzalez Oyarce, T. Trypiniotis, P. E. Roy, and C. H. W. Barnes, Phys. Rev. B **87**, 174408 (2013).

[32] K. Richter, A. Krone, M.-A. Mawass, B. Krüger, M. Weigand, H. Stoll, G. Schütz, and M. Kläui, Phys. Rev. B **94**, 024435 (2016).

[33] K. Richter, A. Krone, M.-A. Mawass, B. Krüger, M. Weigand, H. Stoll, G. Schütz, and M. Kläui, Phys. Rev. Appl. **5**, 024007 (2016).

[34] M.-A. Mawass, K. Richter, A. Bisig, R. M. Reeve, B. Krüger, M. Weigand, H. Stoll, A. Krone, F. Kronast, G. Schütz, and M. Kläui, Phys. Rev. Appl. **7**, 044009 (2017).

[35] C. A. F. Vaz, T. J. Hayward, J. Llandro, F. Schackert, D. Morecroft, J. A. C. Bland, M. Kläui, M. Laufenberg, D. Backes, U. Rüdiger, F. J. Castaño, C. A. Ross, L. J. Heyderman, F. Nolting, A. Locatelli, G. Faini, S. Cherifi, and W. Wensdorfer, J. Phys.: Condens. Matter **19**, 255207 (2007).

[36] F. J. Castano, C. A. Ross, C. Frandsen, A. Eilez, D. Gil, H. I. Smith, M. Redjdal, and F. B. Humphrey, Phys. Rev. B **67**, 184425 (2003).

[37] T. J. Hayward, J. Llandro, R. B. Balsod, J. A. C. Bland, D. Morecroft, F. J. Castaño, and C. A. Ross, Phys. Rev. B **74**, 134405 (2006).

[38] X. Zhu and J.-G. Zhu, IEEE Trans. Magn. **39**, 2854 (2003).

[39] T. Yang, N. R. Pradhan, A. Goldman, A. S. Licht, Y. Li, M. Kemei, M. T. Tuominen, and K. E. Aidala, Appl. Phys. Lett. **98**, 242505 (2011).

[40] N. R. Pradhan, A. S. Licht, Y. Li, Y. Sun, M. T. Tuominen, and K. E. Aidala, Nanotechnology **22**, 485705 (2011).

[41] V. L. Carvalho-Santos, W. A. Moura-Melo, and A. R. Pereira, J. Appl. Phys. **108**, 094310 (2010).

[42] S. Vojkovic, A. S. Nunez, D. Altbir, and V. L. Carvalho-Santos, J. Appl. Phys. **120**, 033901 (2016).

[43] G. R. Lewis, J. C. Loudon, R. Tovey, Y.-H. Chen, A. P. Roberts, R. J. Harrison, P. A. Midgley, and E. Ringe, Nano Lett. **20**, 7405 (2020).

[44] V. L. Carvalho-Santos, A. R. Moura, W. A. Moura-Melo, and A. R. Pereira, Phys. Rev. B **77**, 134450 (2008).

[45] J. Benoit and R. Dandoloff, Phys. Lett. A **248**, 439 (1998).

[46] Y. Gaididei, V. P. Kravchuk, and D. D. Sheka, Phys. Rev. Lett. **112**, 257203 (2014).

[47] A. W. Teixeira, S. Castillo-Sepúlveda, S. Vojkovic, J. M. Fonseca, D. Altbir, A. S. Núñez, and V. L. Carvalho-Santos, J. Magn. Magn. Matter **478**, 253 (2019).

[48] S. Vojkovic, V. L. Carvalho-Santos, J. M. Fonseca, and A. S. Núñez, J. Appl. Phys. **121**, 113906 (2017).

[49] R. G. Elías, N. Vidal-Silva, and V. L. Carvalho-Santos, Sci. Rep. **9**, 14309 (2019).

[50] K. V. Yershov, V. P. Kravchuk, D. D. Sheka, and U. K. Robler, SciPost Phys. **9**, 043 (2020).

[51] V. L. Carvalho-Santos, R. M. Corona, D. Altbir, and S. Castillo-Sepúlveda, Phys. Rev. B **102**, 024444 (2020).

[52] V. P. Kravchuk, D. D. Sheka, A. Kákay, O. M. Volkov, U. K. Rößler, J. van den Brink, D. Makarov, and Y. Gaididei, Phys. Rev. Lett. **120**, 067201 (2018).

[53] P. J. Ackerman and I. I. Smalyukh, Phys. Rev. X **7**, 011006 (2017).

[54] R. Voinescu, Jung-Shen B. Tai, and I. I. Smalyukh, Phys. Rev. Lett. **125**, 057201 (2020).

[55] N. Vidal-Silva, A. Riveros, F. Tejo, J. Escrig, and D. Altbir, Appl. Phys. Lett. **115**, 082405 (2019).

[56] X. S. Wang, A. Qaiumzadeh, and A. Brataas, Phys. Rev. Lett. **123**, 147203 (2019).

[57] M. J. Donahue and D. G. Porter, OOMMF User's Guide, Version 1.0, Interagency Report NISTIR 6376, National Institute of Standards and Technology, Gaithersburg, MD, 1999.

[58] M. Beg, R. Carey, W. Wang, D. Cortés-Ortuño, M. Vousden, M.-A. Bisotti, M. Albert, D. Chernyshenko, O. Hovorka, R. L. Stamps, and H. Fangohr, Sci. Rep. **5**, 17137 (2015).

[59] See Supplemental Material at http://link.aps.org/supplemental/10.1103/PhysRevB.104.184406 for videos showing the full magnetization reversal process for the hopfion, pinned-hopfion, transversal radial wall, and quasicoherent mechanisms.

[60] M. A. Castro, A. P. Espejo, N. M. Vargas, D. Altbir, S. Allende, and V. L. Carvalho-Santos, J. Magn. Magn. Matter **484**, 55 (2019).

[61] W. A. Moura-Melo, A. R. Pereira, R. L. Silva, and N. M. Oliveira-Neto, J. Appl. Phys. **103**, 124306 (2008).

[62] R. L. Silva, A. R. Pereira, R. C. Silva, W. A. Moura-Melo, N. M. Oliveira-Neto, S. A. Leonel, and P. Z. Coura, Phys. Rev. B **78**, 054423 (2008).

[63] X. S. Gao, A. O. Adeyeye, and C. A. Ross, J. Appl. Phys. **103**, 063906 (2008).

[64] P. J. Ackerman and I. Smalyukh, Nat. Mater. **16**, 426 (2017).